PHYSICAL REVIEW B **78**, 081403(R) (2008)

Direct visualization of charge distributions during femtosecond laser ablation of a Si (100) surface

Christoph T. Hebeisen, Germán Sciaini, Maher Harb, Ralph Ernstorfer, Sergei G. Kruglik, and R. J. Dwayne Miller*
Institute for Optical Sciences and Departments of Chemistry and Physics, University of Toronto, 80 St. George Street, Toronto, Ontario M5S 3H6, Canada

(Received 8 May 2008; revised manuscript received 8 July 2008; published 14 August 2008)

We directly observe the charge distributions and resulting electric fields present during the earliest stages of laser ablation of a Si (100) surface by using femtosecond electron pulses as a probe. We find the magnitude of the field to be 3.5×10^{6} V/m just 3 ps after an excitation pulse of 5.6 J/cm^2. By fitting the data to a simple model, we determine that the excitation results in the rapid emission of 5.3×10^{11} electrons/cm^2. These experiments provide new insights into the nature of the ablation process and the behavior of charged particles involved in it.

DOI: 10.1103/PhysRevB.78.081403 PACS number(s): 52.38.Ph, 41.75.−i, 52.70.−m

Femtosecond laser ablation of solids has attracted much attention due to its applications in laser micromachining,[1] laser surgery,[2] and matrix-assisted laser desorption.[3] There are many different processes that lead to the removal of material after excitation with an intense laser pulse. These processes largely fall into two categories.[4] Thermal processes happen after energy relaxation between the electrons and the lattice has taken place. Melting, evaporation, phase explosion, and thermal plasma generation are examples of thermal processes. In nonthermal ablation processes, disintegration of the lattice occurs before the electrons and the lattice have reached thermal equilibrium. Nonthermal processes include nonthermal melting and Coulomb explosion.

Transient electric fields play an important role in different ablation processes. When an intense laser pulse hits the surface of a solid, multiphoton photoemission, avalanche, and field ionization lead to the emission of large numbers of electrons and charging of the surface. Electron escape, recapture, ion emission, and transport processes within the solid modify the spatial charge distributions and the resulting electric fields over time. The trajectories of electrons and ions emitted during ablation are subject to these fields. It should be noted that even below the ablation threshold of a given material, large numbers of electrons can be emitted from a sample. Over time, the positive counter charge on the sample is compensated by recapture of some of the emitted electrons and influx of electrons from nonexcited parts of the sample.[5] Because of electron recapture, the magnitude of the initially emitted charge is often underestimated. However, a transient electron deficit can lead to equally transient changes in the material properties of the excited sample, a fact often ignored in ultrafast high-excitation experiments, which could lead to incorrect interpretations of measurements.

Usually, ablation is studied by analyzing the energy, charge, and direction of the produced electrons, ions, and neutral particles using time-of-flight or other mass spectrometry methods.[4,6–8] These methods yield valuable data allowing identification of different ablation regimes and—assuming a model for the ablation process—certain parameters of the actual process to be extracted. However, most measurements inherently integrate over the ultrashort time scales of the microscopic processes during ablation and as a result, the dynamics have to be implied from a model or need to be determined using a different method. Alternative all-optical methods such as time-resolved shadowgraphy[9,10] can detect ablation plumes in a time-resolved manner but are not sensitive to electrical charge. Okano and coworkers[11] used electron pulses to detect electric fields. The temporal resolution of their study was limited by the 64 ps duration of the electron probe pulses. In this paper, we present a method for the visualization of transient electric fields with temporal resolution on the subpicosecond timescale. This is achieved by using a femtosecond electron pulse to probe the charge distribution. This technique opens the door to a more detailed view of the ablation process since it allows insights into the spatial distributions and behavior of charged particles at the earliest stages of ablation.

The experimental setup is derived from a femtosecond electron diffraction pump-probe setup described in detail elsewhere.[12] A 780 nm, 200 fs laser pulse is split into two arms by a beam splitter. The pulse in one arm (the pump pulse) is frequency doubled by a β-Barium-Borate crystal and focused on the sample surface. The second arm drives a noncollinear optical parametric amplifier whose visible light output is delayed by a variable delay stage and then used to drive the femtosecond electron gun, which is capable of producing electron pulses as short as 200 fs containing thousands of electrons.[13] The vacuum in the sample chamber is better than 10^{-7} Torr. The sample is placed inside the beam path of the electron pulse so that it partially blocks the beam (Fig. 1). The laser pump pulse is aligned to strike the sample surface at normal incidence inside the electron beam trace on the sample surface. The probe electrons in the unblocked part of the electron beam pass the excited sample surface at close distance. Transient electric fields present when the probe pulse passes the sample impart momentum on the probe electrons, which impacts their spatial distribution at the detector. We obtain a time series of the resultant probe electron distributions by repeating this measurement for different pump-probe delays. Each of these images is a snapshot containing information about the electric field present at the exact moment when the electron pulse passed the excited part of the sample.

The sample we used in this study is a strip of Si, produced

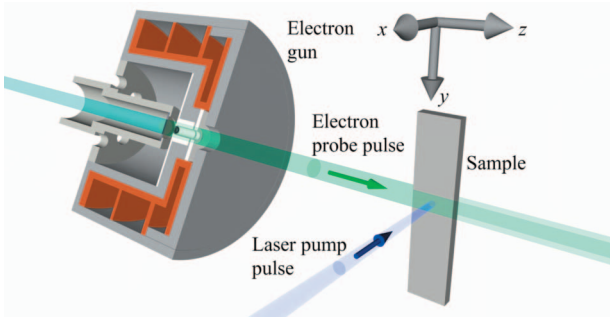

FIG. 1. (Color) When the laser pulse hits the photocathode it produces an electron bunch, which is then accelerated to 55 keV by a dc electric field. The sample is mounted on an *xy* translation stage and placed in the beam path of the electron pulse. The electron distribution is detected using a microchannel plate/phosphor screen detector and recorded by a CCD camera.

from a commercial Si wafer with a 40 nm silicon nitride layer deposited on both sides. Stripe features were patterned in the silicon nitride layer using photolithography and reactive ion etching. This was followed by wet etching in KOH to produce strips of Si. Finally, the nitride layer was removed using 10:1 buffered oxide etch and the sample surface was cleaned with methanol. The resulting Si strips were 330 μm thick. The excitation laser pulse had a wavelength of 390 nm, a duration of 150 fs, and the beam size was 17 μm full width at half maximum (FWHM) at the sample position. Selected images from the time series are shown in Fig. 2. Each beam image was integrated over 40 shots and ablation was observed at all fluences. Hence, surface contamination has no significant effect on these experiments. The sample was moved vertically to a new position for each image. The detected electron intensity remained constant over the time series.

Qualitatively, we interpret the beam shapes shown in Fig. 2 as follows: The probe electrons that pass near the excited part of the sample are initially strongly deflected away from the sample surface due to the emission of a large number of electrons. Despite the attraction of the countercharge on the surface, electrons which are sufficiently far away from the sample surface experience a net force in the opposite direction due to space charge of the emitted electron cloud.[5] By 9.5 ps, this self-acceleration has caused the electron cloud to expand so far that the probe beam is split into two lobes. The

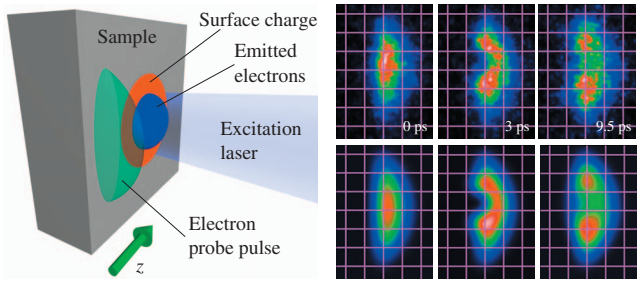

FIG. 3. (Color) Schematic view of the charge distribution model used to fit the data (left) and measured and calculated probe beam maps (right). Experimental beam maps are shown in the top row, the corresponding fit results using the model are shown in the bottom row.

probe electrons above and below the excitation spot are deflected into the sample shadow by the attractive field of the counter charge. This deflection toward the sample becomes more and more pronounced at 30 ps and 100 ps. However, a localized electron cloud still partially shields the Coulomb attraction to the center part of the probe beam, causing a persistent indentation in the middle of the electron beam profile. As more electrons continue to escape or get reabsorbed, the negative charge density near the surface reduces. At 300 ps and later, the attractive force of the ions clearly dominates.

The momentum change, which a probe electron experiences due to a charge Q at the origin is

$$\Delta\vec{p} = \int \frac{-Qe}{4\pi\varepsilon_0|\vec{r}(t)|^3}\vec{r}(t)dt. \quad (1)$$

Here, $\vec{r}(t)=(x,y,z)$ is the position of the probe electron, e is the elementary charge, and ε_0 is the permittivity of free space. We assume that the charge is not moving in the period during which the probe electron traverses the region of significant electric field caused by the charge. Given the size of the excitation beam (17 μm) and the kinetic energy of the probe electrons (55 keV), the probe electron passes the excited region of the sample in 130 fs. At least at early times, i.e., before the charge distribution has any time to spread significantly beyond the excited region, the assumption of a frozen charge distribution is justified. If the angle of deflec-

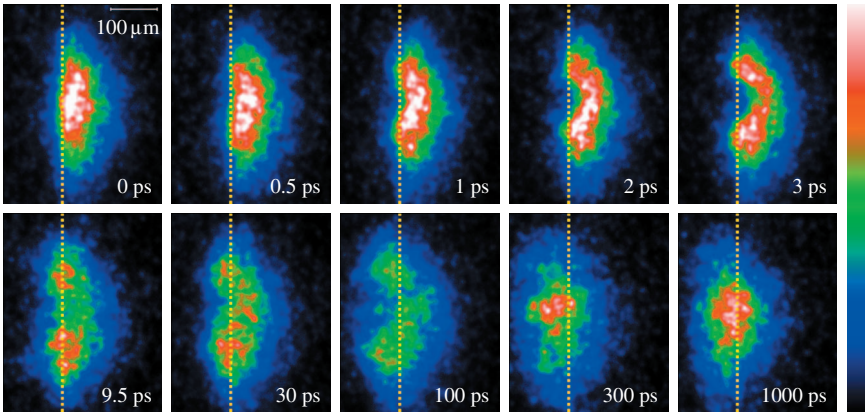

FIG. 2. (Color) Probe electron density maps at the detector. Each frame is averaged over 40 laser shots. In these images, the laser beam is incident from the right side; the sample surface is indicated by the yellow line. The scale indicates size in the sample plane, the image on the detector appears 5.9× larger due to electron beam divergence. Peak laser fluence: 5.6 J/cm^2.

tion and the longitudinal momentum transfer are small, we can rewrite Eq. (1) as

$$\Delta\vec{p} = \frac{-Qe}{4\pi\varepsilon_0 v_z}\int \frac{\vec{r}}{|\vec{r}|^3}dz \tag{2}$$

for an electron initially propagating parallel to the z axis with velocity v_z. The deflection $\Delta(X,Y)$ of the probe electron at the detector is then

$$\Delta(X,Y) = \frac{\Delta(p_x,p_y)l}{m_e v_z} = -\frac{-Qel}{2\pi\varepsilon_0 m_e v_z^2}\frac{(x,y)}{(x^2+y^2)}, \tag{3}$$

where m_e is the mass of the electron and l is the length of the drift region, i.e., the distance between the sample and the detector. If the charge distribution is concentrated in a short section along the electron beam path, we can integrate Eq. (3) over the charge distribution to calculate the cumulative effect that the charge distribution has on the probe electrons.

While this allows us to calculate the positions of probe electrons on the detector for a given charge distribution at the sample, we cannot calculate the charge distribution from the detected electron beam shapes because the "origin" (x,y) of an electron detected in a given detector position (X,Y) cannot be determined. Imperfections of the electron beam further complicate the interpretation of the acquired images by introducing image blur.

A full quantitative model of the ablation process treating free electrons and carriers in the sample could be used to predict the probe beam images. In this respect, these experiments could serve as a direct qualitative, as well as quantitative, test. Lacking a detailed microscopic model, we fit the experimental data using a phenomenological model, which makes no assumptions about dynamics. The model charge distribution consists of two parts: positive charges on the sample surface and a cloud of emitted electrons above the surface (see Fig. 3). Both parts of the charge distributions are radially symmetric around the x axis and the model assumes that the radial distributions are Gaussian. The positive charge on the sample is contained in a plane on the sample surface while the electron density in the charge cloud near the sample falls off exponentially with increasing distance from the surface. The probe beam shape resulting from this charge distribution was calculated to fit every time delay separately. The parameters of the fit were the amount of positive charge on the sample surface Q_s, the radial size (FWHM) of that charge distribution H_s, the thickness $(1/e)$ of the electron cloud in front of the sample surface W_c, and the radial size of that electron cloud H_c. The vertical position of the two charge distributions Y_s had to be fit as well in order to compensate for electron beam pointing instability. The amount of charge in the electron cloud Q_c was set to $-Q_s$. In fits we performed with Q_c as an independent fit parameter, Q_s+Q_c was consistent with 0 for the range of delay times for which the fits delivered meaningful results but the outcome of the fits was more noisy. A genetic search algorithm[14] was used to perform the fits. Since this model assumes a static charge distribution for each time step it cannot include magnetic fields. However, the magnetic fields caused by the dynamics seen in the fit results would not have any significant effects on the probe electron distribution.

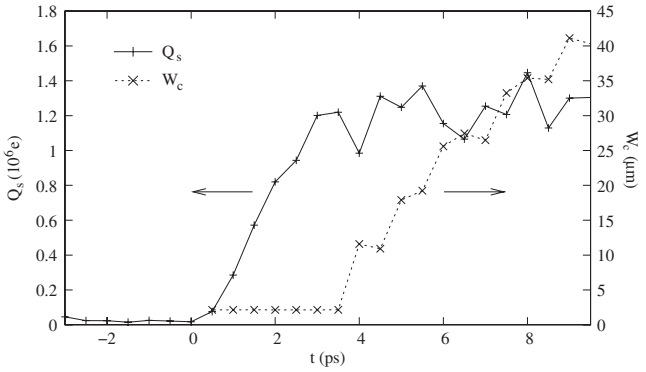

FIG. 4. Total amount of positive charge on the sample Q_s and width of the electron cloud W_c vs time. Data points for W_c before $t=0$ have been omitted as they have no meaning in the absence of charge, i.e., before the laser excitation.

The model obviously places restrictions on the shapes of the involved charge distributions and ignores escaping electrons, emitted ions, and charge refilling from the bulk. While all of these effects modify the charge distribution after some time, the model can still deliver an estimate of the size of the charge distributions, as well as the amount of charge for times shortly after excitation. Up to about 10 ps, the experimental results are reproduced well by fits to this model. Measured and fitted beam images are shown in Fig. 3. We believe that the deviations for later times are caused by the escape of some of the emitted electrons well beyond the envelope of the probe beam, as well as shortcomings of the assumptions about the charge density distributions in our model. We attempted to add a separate escaping charge distribution to the above model; however, the large number of parameters, some of them with weak dependence, made the fits unstable.

The time series of Q_s and W_c are shown in Fig. 4. The emission of electrons starts at $t=0$, which was expected since the onset of change in the electron probe beam was used as the $t=0$ marker for this experiment. The amount of emitted charge reaches a plateau after 3 ps, after which W_c starts to grow rapidly. The speed of this expansion of the electron cloud is about 2% of the speed of light corresponding to a kinetic energy of 100 eV. The model does not treat crater formation of the multishot ablation process. Crater formation may contribute to the delay in the rise of W_c and lead to an underestimation of Q_c, especially at early times. After this paper was submitted for review, we learned of a study[15] which used electron pulses to study plasma generation by a femtosecond laser pulse in a nitrogen gas jet. The temporal resolution of these experiments is limited to several picoseconds by the duration of the electron pulses and the velocity mismatch between the laser pump and electron probe pulses. An electron temperature of 250 eV was observed.

A much simpler analysis of the probe beam images allows us to calculate the average electric field in x direction $\langle E_x\rangle$ experienced by the probe electrons over their path through the charge distribution. Using Eq. (3), the average deflection $\langle\Delta X\rangle$ is

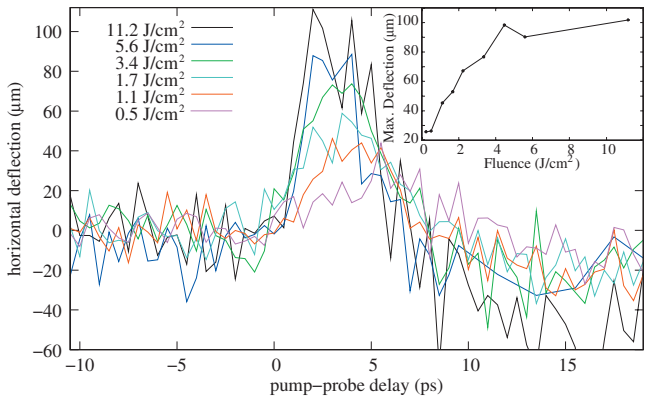

FIG. 5. (Color) Probe electron deflection for different laser fluences. The main graph shows the time dependence of the probe deflection, whereas the inset shows the maximum deflection for each fluence as determined by a Gaussian fit to the deflection time trace.

$$\langle \Delta X(t) \rangle = \frac{l}{v_z} \times \frac{\Delta p_x}{m_e} = \frac{le\langle E_x(t)\rangle d_z}{v_z^2 m_e}, \tag{4}$$

where d is the distance along z over which the electric field acts on the probe electron. The size of the "dent" in the probe electron distribution at 3 ps is $d_y = 16$ μm in y direction (very close to the laser beam size) and for symmetry reasons, $d_z = d_y$. Time traces of $\langle \Delta X \rangle$ at the center of the probe beam for a range of excitation fluences are shown in Fig. 5. Using the measured maximum deflection at 5.6 J/cm^2, $\langle \Delta X(3 \text{ ps}) \rangle = 108$ μm we obtain $\langle E_x \rangle = 3.5 \times 10^6$ V/m for the electric field at this point in space and time.

For fluences above 1.7 J/cm^2, $\langle \Delta X \rangle$ peaks at the same time. At 1.1 J/cm^2, the peak is clearly delayed, an effect even more obvious at 0.5 J/cm^2. The plasma formation threshold[6] for 100 fs, 620 nm pulses is ≈ 1 J/cm^2. Below this threshold, ablation occurs through the emission of neutrals. As opposed to the massive ionization through avalanche ionization or field ionization, which occurs at higher fluences, only a moderate number of electrons is emitted through multiphoton photoemission for excitation below the plasma formation threshold. The lower number of emitted electrons also results in weaker self-acceleration of the emitted electron cloud. The amplitude of the deflection increases with the intensity of the incident laser pulse, however there appears to be a saturation value which is reached for excitations above 4 J/cm^2.

In summary, we have observed the transient charge distributions produced during femtosecond laser ablation from a Si (100) surface on the subpicosecond time scale. We determined the electric field strength from the maximum deflection of the probe electrons (3.5×10^6 V/m for 5.6 J/cm^2 pump fluence). Fits to a simple charge distribution model reveal that this field is produced by the emission of 1.2×10^6 electrons (5.3×10^{11} electrons/cm^2). According to calculations,[16] the initiation of Coulomb explosion (CE) in Si requires the emission of on the order of 10^{14} electrons/cm^2. Direct plasma generation, on the other hand, is estimated[17] to happen at a free electron density of 10^{12} cm^{-2} nm^{-1}. Given that only a fraction of these electrons are expected to escape, our results are consistent with the latter, as expected in a multipulse ablation scenario. While there is some evidence for the occurrence of CE in semiconductors,[4,8] its role has been disputed.[18,19] By using only one or few pulses per sample position, the method presented in this paper is capable of distinguishing the different ablation processes and can be used to determine if CE exists as an ablation pathway for semiconductor surfaces. It will be interesting to extend this approach to different materials and a range of different laser fluences. Preliminary data using a metal surface and higher excitation show significantly faster dynamics. This approach can provide information for the development of more efficient laser ablation processes for numerous analytical measurements and material processing applications. With a detailed microscopic theory, these experiments will enable effectively a direct observation of the dynamics of the charges emitted in the ablation process.

The authors wish to acknowledge R. Loo (University of Toronto) for AFM support. This work was funded by the Natural Science and Engineering Research Council of Canada.

*dmiller@lphys.chem.utoronto.ca

[1] C. Y. Chien and M. C. Gupta, Appl. Phys. A: Mater. Sci. Process. **81**, 1257 (2005).
[2] A. Vogel *et al.*, Appl. Phys. B: Lasers Opt. **81**, 1015 (2005).
[3] R. Knochenmuss, Analyst (Cambridge, U.K.) **131**, 966 (2006).
[4] H. Dachraoui *et al.*, Appl. Phys. A: Mater. Sci. Process. **83**, 333 (2006).
[5] T. L. Gilton *et al.*, J. Appl. Phys. **68**, 4802 (1990).
[6] A. Cavalleri *et al.*, J. Appl. Phys. **85**, 3301 (1999).
[7] R. Stoian *et al.*, Phys. Rev. B **62**, 13167 (2000).
[8] W. G. Roeterdink *et al.*, Appl. Phys. Lett. **82**, 4190 (2003).
[9] N. Zhang *et al.*, Phys. Rev. Lett. **99**, 167602 (2007).
[10] J. König *et al.*, Opt. Express **13**, 10597 (2005).
[11] Y. Okano *et al.*, Appl. Phys. Lett. **86**, 141501 (2005).
[12] J. R. Dwyer *et al.*, Philos. Trans. R. Soc. London, Ser. A **364**, 741 (2006).
[13] C. T. Hebeisen *et al.*, Opt. Express **16**, 3334 (2008).
[14] D. Zeidler *et al.*, Phys. Rev. A **64**, 023420 (2001).
[15] M. Centurion *et al.*, Nat. Photonics **2**, 315 (2008).
[16] W. Marine *et al.*, J. Appl. Phys. **103**, 094902 (2008).
[17] B. C. Stuart *et al.*, Phys. Rev. B **53**, 1749 (1996).
[18] N. M. Bulgakova *et al.*, Phys. Rev. B **69**, 054102 (2004).
[19] R. Stoian *et al.*, Appl. Phys. Lett. **85**, 694 (2004).